

Spin-wave excitations of an emergent skyrmion crystal in manganite-iridate oxide interfaces*

Narayan Mohanta,¹ Andrew D. Christianson,¹ Satoshi Okamoto,¹ and Elbio Dagotto^{1,2}

¹*Material Science and Technology Division, Oak Ridge National Laboratory, Oak Ridge, TN 37831, USA*

²*Department of Physics and Astronomy, The University of Tennessee, Knoxville, TN 37996, USA*

The two-dimensional metallic interface between lanthanum manganite and strontium iridate is a prototypical platform for the realization of a triangular crystal of Néel-type skyrmions at low temperatures in the presence of an external magnetic field, applied perpendicular to the interface. The skyrmion crystal is stabilized by the Dzyaloshinskii-Moriya -type anti-symmetric spin-exchange interaction located at the interface due to the broken structural inversion symmetry and strong spin-orbit coupling in the iridate. We investigate spin-wave excitations emerging from the skyrmion crystal by employing the Monte Carlo simulations and Landau-Lifshitz spin-dynamics calculations. The computed dynamical spin structure factor $S(\mathbf{q}, \omega)$ reveals that six modes of spin-wave excitations appear in the skyrmion crystal at low temperatures and are supplemented by the spin-wave mode coming from the zero-momentum magnetic ordering of the ferromagnetic background. Above the critical temperature T_s for the skyrmion crystallization, we find a diffusive regime of temperatures that confirms previous experimental findings that skyrmionic correlation starts to develop above T_s as the precursor of the long-range skyrmion crystal order. We also explore the spin-wave excitations originating from the spin spiral phase that is stabilized spontaneously at zero magnetic field. We discuss the challenges and opportunities for the experimental detection of these spin-wave excitations of the skyrmion crystal in inelastic neutron-scattering experiments based on multi-layer superlattices of the manganite-iridate heterostructure.

I. INTRODUCTION

Chiral magnetic order occurring in several Condensed Matter systems has added a new dimension to the realization of novel functionalities and exotic fundamental physics [1, 2]. Magnetic skyrmions, the vortex-like spin swirls, belong to the class of chiral magnetic textures having a quantized topological charge [3]. In the presence of competing spin exchange interactions, the skyrmions often arrange themselves naturally in a triangular array to form a skyrmion crystal (SkX) in position space [4–7]. The existence of the SkX phase has been established in a surge of recent experiments by Lorentz transmission electron microscopy, spin-resolved scanning tunneling microscopy, and elastic small-angle neutron scattering (SANS) [8–17]. A magnetic skyrmion generates an emergent electro-magnetic field [18, 19], giving rise to topological Hall effect in metals. This effect also serves as an indirect yet effective probe for the chiral magnetic order in the SkX phase [20–31].

At the interface between the ferromagnetic metal $\text{La}_{1-x}\text{Sr}_x\text{MnO}_3$ ($0.2 \lesssim x \lesssim 0.5$) and the non-magnetic

semimetal SrIrO_3 , the SkX phase is expected to be stabilized within a range of magnetic fields because of the presence of Dzyaloshinskii-Moriya interaction (DMI) [32–34]. The DMI arises at the interface between these two oxide compounds due to the strong spin-orbit coupling in SrIrO_3 and the broken inversion symmetry at the interface [35, 36]. The skyrmions at oxide interfaces are expected to be Néel-type, different from the Bloch-type skyrmions observed in chiral magnets [8, 9], because the Dzyaloshinskii-Moriya vectors predominantly reside at the interfacial plane [37]. The presence of a SkX phase has been inferred in various oxide interfaces via topological Hall effect experiments [37–39]. Recent SANS experiments, revealing the existence of an ordered crystal of magnetic skyrmions in thin multilayer Fe/Gd films [40], opened up opportunities for a similar detection of the SkX phase using multilayer heterostructures made of the two oxide compounds under consideration.

The SkX phase exhibits spin-wave excitations which are Goldstone modes associated with the chiral spin arrangement of the state. The dispersion of these spin-wave modes is determined by the properties of the SkX. Three SkX spin-wave modes – *viz.* clockwise, counterclockwise circulation and breathing modes – have been predicted in previous theoretical analysis [41–43] and subsequently reported in experiments using broadband microwave spectroscopy [44–46]. The motivation of the present study lies in the fact that an effective means for studying the spin-wave excitations in the SkX phase is using the inelastic SANS measurements to map broad regions of momentum (\mathbf{q}) and energy (ω) space directly. Therefore, the investigation of the experimentally observable $S(\mathbf{q}, \omega)$, the dynamical spin structure factor, is important to understand in depth the SkX phase.

* Copyright notice: This manuscript has been authored by UT-Battelle, LLC under Contract No. DE-AC05-00OR22725 with the U.S. Department of Energy. The United States Government retains and the publisher, by accepting the article for publication, acknowledges that the United States Government retains a non-exclusive, paid-up, irrevocable, world-wide license to publish or reproduce the published form of this manuscript, or allow others to do so, for United States Government purposes. The Department of Energy will provide public access to these results of federally sponsored research in accordance with the DOE Public Access Plan (<http://energy.gov/downloads/doepublic-access-plan>).

In this work, we theoretically investigate the spin-wave excitations of the SkX phase, expected to be realized at oxide interfaces involving $\text{La}_{1-x}\text{Sr}_x\text{MnO}_3$ and SrIrO_3 , by computing the dynamical spin structure factor $S(\mathbf{q}, \omega)$ expecting its future direct measurement in inelastic SANS experiments. We use a spin Hamiltonian to first find out the stable spin configurations at low temperatures using the Metropolis Monte Carlo annealing method and then numerically solve the Landau-Lifshitz equation of motion to capture the spin dynamics. The computed $S(\mathbf{q}, \omega)$ reveals an exotic array of six gapless spin-wave modes in the SkX phase, stabilized within a range of the external perpendicular magnetic fields, accompanied by another gapless mode originating from the ferromagnetic background. The spin spiral (SS) phase, which is the natural solution at zero magnetic field, exhibits two gapless spin-wave modes from the spiral order and a soft ferromagnetic mode that appears at finite energies and goes away with increasing the DMI strength. The field-polarized ferromagnetic (FM) phase exhibits a spin-wave mode which appears with an excitation gap equal to the magnetic field. The transition from the high-temperature paramagnetic phase to the low-temperature SkX phase at a finite magnetic field evolves through an intermediate diffusive regime in which the non-trivial topological spin-winding appears as a precursor of the SkX phase [47–49]. We explore the diffusive regime for the skyrmion crystallization and confirm the previous experimental findings that the transition to the SkX phase upon cooling slowly from a higher temperature occurs via a precursor regime. The detection of the spin-wave modes in the SkX phase via inelastic scattering experiments possesses both challenges and opportunities. The challenges may come from the small signal to noise ratio from a single interface and it can possibly be overcome by employing multilayer heterostructures. We discuss the feasibility of the experimental detection of our results based on the state-of-the-art SANS spectrometers and we outline the developments required for a successful future confirmation of our predictions. Advances in flux and instrumentation at next generation neutron scattering facilities, that are either planned or under construction, will likely enable these modes to be studied experimentally.

II. RESULTS

Model for the manganite/iridate interface. We consider a two-dimensional interface that contains the essential properties of both the $\text{La}_{1-x}\text{Sr}_x\text{MnO}_3$ and the SrIrO_3 . The manganite is considered to be doped suitably to be in the ferromagnetic phase in which the localized spins can be described effectively by a Heisenberg exchange interaction. The influence of the strong spin-orbit coupling of the iridate, in the absence of explicit structural inversion symmetry, leads to the DMI at the interface. The total Hamiltonian, in the presence of an

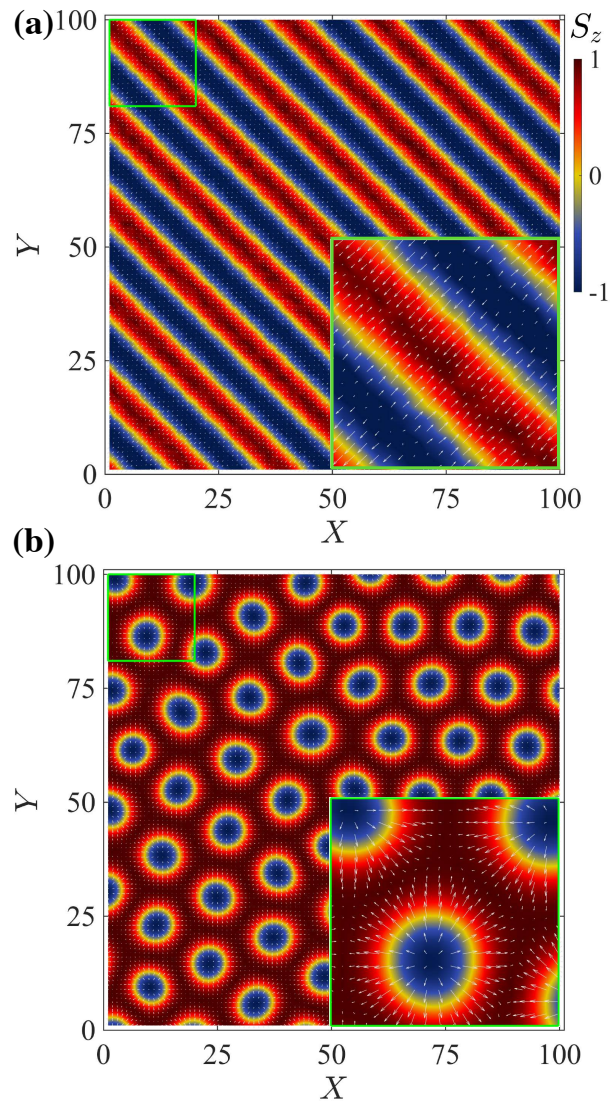


FIG. 1. **Spin textures in the SS and the SkX phases.** The spin textures were spontaneously generated in the Monte Carlo annealing process in a 100×100 square lattice with periodic boundaries: (a) SS texture realized at zero magnetic field ($H_z = 0$), (b) nearly-triangular crystal of skyrmions realized at a magnetic field $H_z = 0.18J$ (≈ 3.74 T). Parameters used are $J = 1$, $S = 3/2$, $D = 0.5J$, $A = 0.01J$ and $T = 0.001J$ (≈ 14 mK). The white arrows and the colorbar respectively show the in-plane (x and y) components and the perpendicular (z) component of the spins. The insets show an expanded view of the spin configuration inside the region denoted by the green square on the top-left corner.

external magnetic field, is given by

$$\begin{aligned} \mathcal{H} = & -J \sum_{\langle ij \rangle} \mathbf{S}_i \cdot \mathbf{S}_j - D \sum_{\langle ij \rangle} (\hat{z} \times \hat{r}_{ij}) \cdot (\mathbf{S}_i \times \mathbf{S}_j) \\ & - H_z \sum_i S_{zi} - A \sum_i |S_{zi}|^2, \end{aligned} \quad (1)$$

where J is the nearest-neighbor ferromagnetic exchange parameter, D is the DMI strength, H_z is the magnetic

field applied perpendicular to the interfacial plane, and A_z is the easy-plane magnetic anisotropy originating from the combined interfacial strain and Rashba spin-orbit coupling [50]. We used $A = 0.01J$ throughout this paper. \mathbf{S}_i is the localized spin of amplitude $S = 3/2$ on the Mn t_{2g} orbitals at site i on the manganite side of the interface. By comparing the critical temperature for the zero-field FM phase (at $D = 0$) extracted from our Hamiltonian with the experimental findings [33], it was found that the Heisenberg exchange energy constant at the manganite/iridate films varies within the range $1.2 \text{ meV} \lesssim J \lesssim 3.9 \text{ meV}$, depending upon the thickness of the film [32]. In the description below, we present energies in units of J and reveal magnetic field and temperature scales, at selected places, using $J = 1.2 \text{ meV}$.

Low-temperature spin configurations. We present the spin-wave excitations, obtained using a 100×100 lattice at different magnetic fields, first at a fixed temperature $T = 0.001J$ and then discuss the finite-temperature diffusive regime of SkX formation. The SS phase, which is stabilized at zero magnetic field, evolves into a triangular SkX within a range of magnetic fields and finally becomes a fully-polarized FM phase at higher fields. A detailed analysis of the phase diagram, spanned by the magnetic field and the temperature, was done in our previous work [32]. In Fig. 1(a) and (b), we show the spin configurations of the SS phase and the SkX phase, obtained in a typical annealing session of the Monte Carlo simulations, respectively at zero field ($H_z = 0$) and at a finite field ($H_z = 0.18J$). Since the DM vectors lie predominantly at the interface plane, the SS and the SkX textures are Néel-type in nature, unlike in three-dimensional chiral magnets such as MnSi in which out-of-plane DM vectors lead to Bloch-type textures. A change in the sign of D reverses the sense of rotation of the spins in going from the skyrmion center towards the radially outward direction. At the considered DMI strength $D = 0.5J$, which is close to the value realizable at oxide interfaces [37], the period of the SS and the skyrmion diameter are nearly 12 lattice spacings. At smaller values of D , these length scales increase almost exponentially, $D = 0$ ($H_z = 0$) being the rotationally-invariant Heisenberg FM phase.

Spin waves in the field-polarized ferromagnet. We begin with the analysis of the spin-wave excitation in the FM phase which is realized at a magnetic field $H_z = 0.5J$ in the MC simulations. Figure 2(a) shows the dynamical spin structure factor $S(\mathbf{q}, \omega)$ computed along a momentum path $\Gamma(0, 0) - X(\pi, 0) - M(\pi, \pi) - \Gamma$ in the Brillouin zone. The plot describes the well-known spin-wave dispersion relation $\omega = H_z + 4JS(\cos q_x + \cos q_y)$ with a bandwidth $\sim 12J$ and an energy gap $\Delta\omega = 0.5J$. Figures 2(b)-(e) show the constant-energy contours of the spin-wave dispersion at different energies. The point-like peak in $S(\mathbf{q}, \omega)$ at the Γ point at energy $\omega = 0.5J$ evolves into a

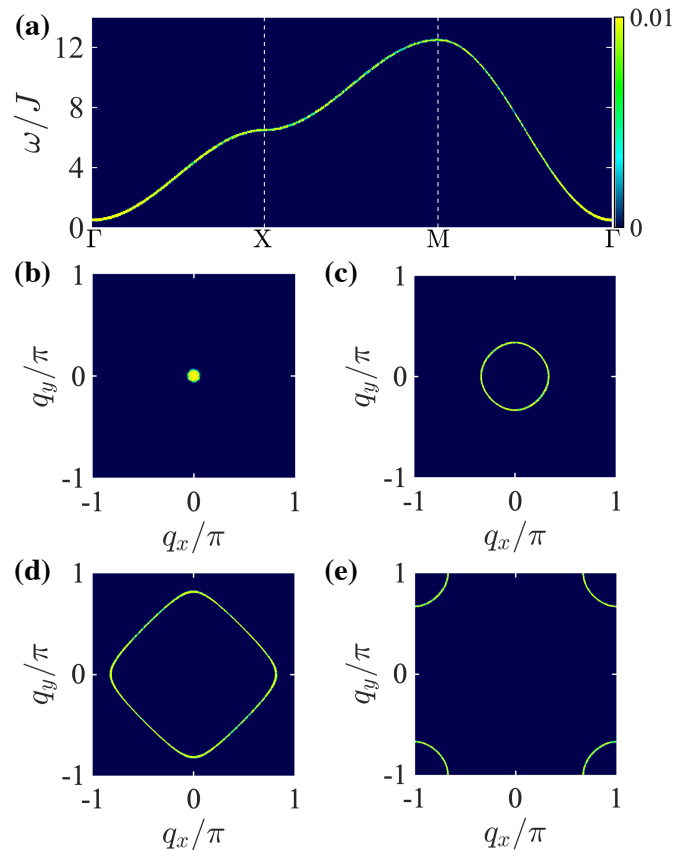


FIG. 2. **Spin waves in the field-polarized FM phase.** (a) The dynamical spin structure factor $S(\mathbf{q}, \omega)$ calculated in the FM phase, realized at a magnetic field $H_z = 0.5J$ ($\approx 10.37 \text{ T}$), along the momentum path $\Gamma(0, 0) - X(\pi, 0) - M(\pi, \pi) - \Gamma$. Plots (b) to (e) show the constant-energy contours of $S(\mathbf{q}, \omega)$ at energies (b) $\omega = 0.5J$, (c) $\omega = 2J$, (d) $\omega = 6J$, and (e) $\omega = 11J$. Other parameters used are the same as in Fig. 1.

circle with increasing ω and the circle takes the shape of a rounded square at $\omega \approx 6J$. With further increase in ω , the topology of the energy contour changes (characteristic of the Lifshitz transition) and four hole-like pockets appear at the corners of the Brillouin zone. These hole pockets disappear above the upper limit, $\omega \approx 12.5J$, of the energy spectrum.

The sharpness of the $S(\mathbf{q}, \omega)$ dispersion in the frequency-momentum space is controlled primarily by the lattice size and the time step. At smaller lattice sizes, the $S(\mathbf{q}, \omega)$ peaks appear discontinuously along the dispersion curve. With larger lattice sizes, the increase in the number of peaks form a continuous sharply-defined curve. An analysis of finite-size effects on the spin-wave dispersion was done in Ref. 51. On the other hand, a larger time step introduces tails along the ω axis surrounding the peak positions with an amplitude that decays in an oscillatory manner with distance from the ω of the peak. A sufficiently small time step reduces these tails significantly from the dispersion curve. In three-dimensional materials with a finite DMI, the fully-polarized FM phase at a finite magnetic field

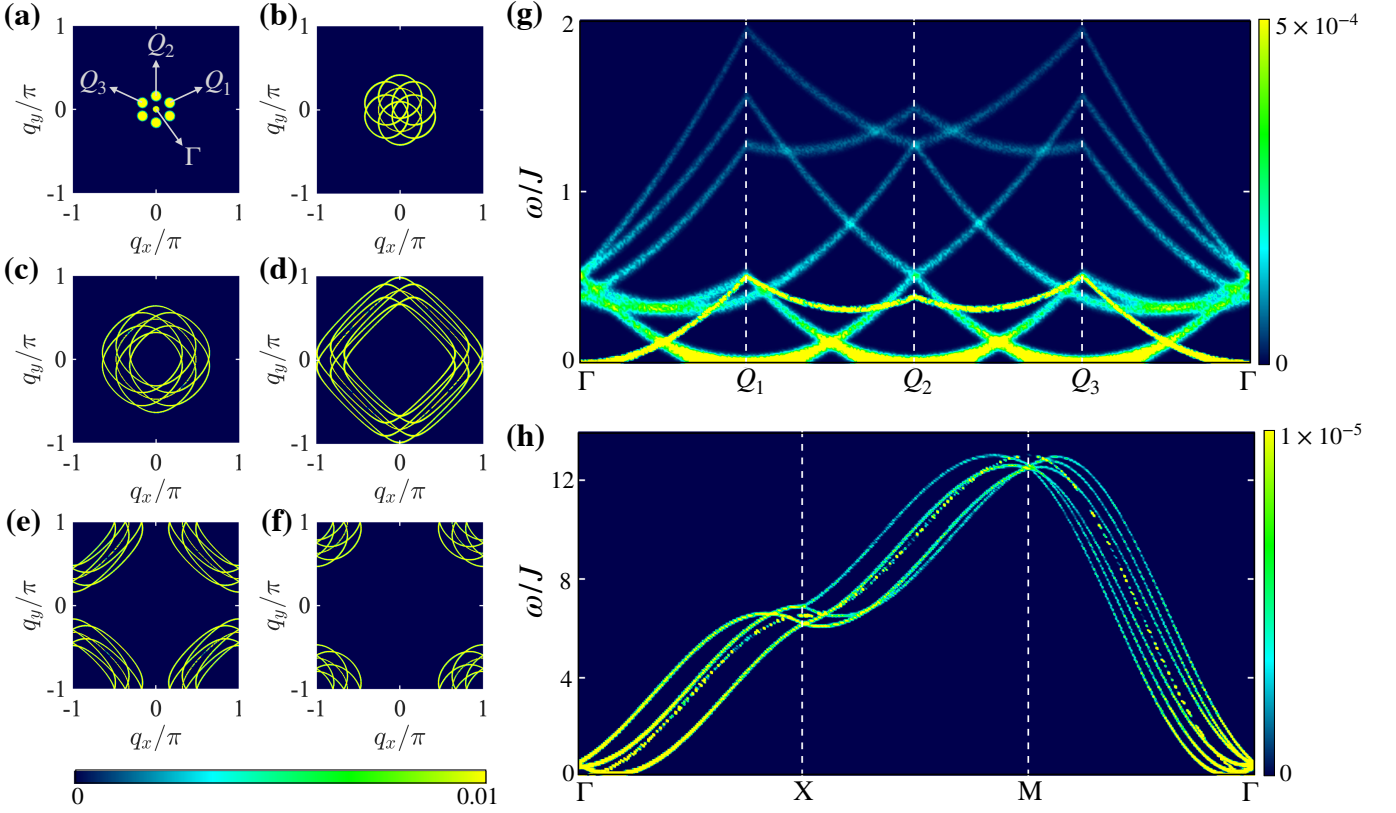


FIG. 3. **Spin waves in the SkX phase.** (a)-(f) Constant-energy contours of the dynamical spin structure factor $S(\mathbf{q}, \omega)$ calculated in the SkX phase, realized at a magnetic field $H_z = 0.18J$ (≈ 3.74 T), at energies (a) $\omega=0$, (b) $\omega=J$, (c) $\omega=3J$, (d) $\omega=6J$, (e) $\omega=8J$, and (f) $\omega=11J$. Plot (a) shows the three characteristic momenta \mathbf{Q}_1 , \mathbf{Q}_2 and \mathbf{Q}_3 of the SkX. (g)-(h) Plots of $S(\mathbf{q}, \omega)$ along the momentum paths (g) $\Gamma - \mathbf{Q}_1 - \mathbf{Q}_2 - \mathbf{Q}_3 - \Gamma$ and (h) $\Gamma - X - M - \Gamma$. The spin-wave mode originating from the Γ (0,0) point is due to the ferromagnetic background in the SkX. The rest six branches arise from the triangular SkX spin configuration (Fig. 1(b)). Other parameters employed are as in Fig. 1.

exhibits an anisotropy in the spin-wave dispersion, the anisotropy being proportional to the DMI strength D and the perpendicular momentum k_z [43, 52]. In two dimensions, the anisotropy goes away and the spin-wave dispersion is similar to a two-dimensional ferromagnet.

Spin waves in the skyrmion crystal. As the magnetic field is reduced from the field-polarized FM phase, isolated skyrmions start to appear within the FM background, leading to a gaseous phase of skyrmions [32]. With further decrease in the magnetic field, the skyrmions form a triangular crystal. At the DMI strength $D = 0.5J$, the SkX phase was realized within the field range $0.13J \lesssim H_z \lesssim 0.20J$. We focus on the SkX phase obtained at $H_z = 0.18J$, shown in Fig. 1(b). In Fig. 3(a)-(f), we show the constant-energy contours of the dynamical spin structure factor $S(\mathbf{q}, \omega)$ at different energies. The plot at $\omega=0$ in Fig. 3(a) depicts the six-peak structure of the SkX phase, as revealed in elastic neutron-scattering experiments (see *e.g.* Fig.2E in Ref. 9). The three characteristic momenta of the triangular SkX phase are denoted by \mathbf{Q}_1 , \mathbf{Q}_2 and \mathbf{Q}_3 . The peak at the Γ point originates from the zero-momentum magnetic ordering in the ferromagnetic background of the SkX. The constant-energy

contours of $S(\mathbf{q}, \omega)$ at different finite energies are shown in Fig. 3(b)-(f). At a finite energy $\omega=J$, the seven elastic peaks evolve into circles as shown in Fig. 3(b). With the increase in energy, these circles grow in size and, like in the case of the fully-polarized FM phase, deviate their shape to rounded squares near energy $\omega=6J$ (Fig. 3(d)). At much higher energies, seven pockets appear at the corners of the Brillouin zone (Fig. 3(e)) and these modes disappear at energies above $\omega \approx 13J$.

In Fig. 3(g), we present the momentum-energy dependence of $S(\mathbf{q}, \omega)$ of the SkX phase, the main result of the paper, along the high-symmetry path $\Gamma - \mathbf{Q}_1 - \mathbf{Q}_2 - \mathbf{Q}_3 - \Gamma$. The plot unveils a complex structure for the spin-wave modes, six of which originate from the SkX and another from the ferromagnetic background. The spin-wave modes from the SkX appear to follow a parabolic dispersion relation ($\omega \propto q^2$) in the low-energy regime $\omega \lesssim 0.2J$, around each elastic peak. As shown in Fig. 3(h), the spin-wave modes of the SkX along the $\Gamma - X$ direction are two-fold degenerate. The rich features shown in Fig. 3(g) are a remarkable result and its possible experimental confirmation is addressed below.

In the presence of an additional AC magnetic field, three spin-wave modes of the SkX phase were numeri-

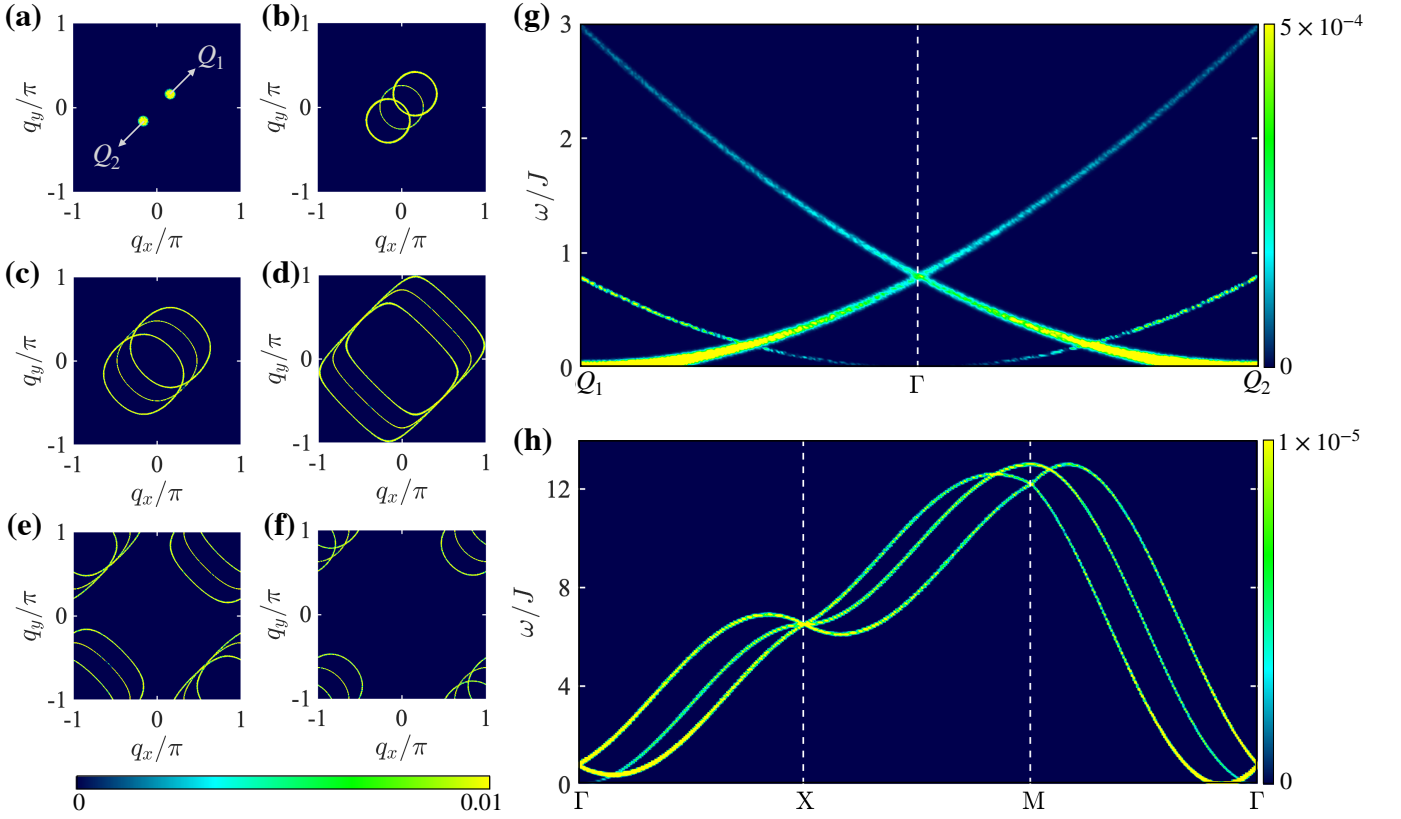


FIG. 4. **Spin waves in the SS phase.** (a)-(f) Constant-energy contours of the dynamical spin structure factor $S(\mathbf{q}, \omega)$ calculated in the SS phase, realized at zero magnetic field, at energies (a) $\omega=0$, (b) $\omega=J$, (c) $\omega=3J$, (d) $\omega=6J$, (e) $\omega=8J$, and (f) $\omega=11J$. \mathbf{Q}_1 ($=-\mathbf{Q}_2$) is the characteristic momentum of the SS phase, as shown in plot (a). (g)-(h) Plot of $S(\mathbf{q}, \omega)$ along the momentum paths (g) $\mathbf{Q}_1 - \Gamma - \mathbf{Q}_2$ and (h) $\Gamma - X - M - \Gamma$. Panel (g) is a symmetrized expansion of the lower right corner of panel (h). The ‘soft’ spin-wave mode, which arises above a finite energy around the Γ point (0,0), is due to the ferromagnetic correlation within the stripes in the SS phase. The two other spin-wave modes arise from the spiral order (Fig. 1(a)). Other parameters are the same as in Fig. 1.

cally identified in Ref. [41]. Two of these three modes are rotational modes (clockwise and counterclockwise) that appear with in-plane AC magnetic field. The third one which was found with out-of-plane AC magnetic field is called the “breathing” mode, where the skyrmion core expands and shrinks alternatively. These modes were subsequently reported in experiments using the broadband microwave spectroscopy in the skyrmion-host compounds MnSi, $\text{Fe}_{1-x}\text{Co}_x\text{Si}$, Cu_2OSeO_3 and GaV_4S_8 [44–46]. We speculate that these three modes correspond to the excitations at energy $\omega \approx 0.5J$ at the Γ point in Fig. 3(g). Previous efforts [42, 43, 53] analytically obtained the spin-wave modes of the SkX that we explore here. Below, we discuss the feasibility of the detection of the spin-wave modes, obtained in our calculations at constant magnetic field, in inelastic neutron-scattering experiments.

Spin waves in the spin spiral. Having explored the spin-wave excitations of the FM and the SkX phases, we next focus on the SS phase that appears spontaneously in the absence of any external magnetic field at low temperatures in our model. The SS phase has a single char-

acteristic momentum \mathbf{Q}_1 that is governed by the period of the spiral texture. It is shown in the constant-energy contour of $S(\mathbf{q}, \omega)$ at $\omega=0$ in Fig. 4(a). With an increase in energy, the two elastic peaks at \mathbf{Q}_1 and $\mathbf{Q}_2 = -\mathbf{Q}_1$, similarly as in the FM and the SkX phases, evolve into circles around these characteristic momenta, as shown by the constant-energy contour of $S(\mathbf{q}, \omega)$ at $\omega = J$ in Fig. 4(b). In addition to the two spin-wave modes of the spiral texture, a soft ferromagnetic mode appears at finite energies, as shown by the circle around the Γ point in Fig. 4(b). The intensity of this ferromagnetic mode decreases with a decrease in the period of the SS texture, *i.e.* with an increase in the DMI strength D . The constant-energy contours of $S(\mathbf{q}, \omega)$ at different energies in Fig. 4(c)-(f) show the spin-wave modes behaving in a similar manner as in the FM or in the SkX phase.

We show the momentum–energy dependence of $S(\mathbf{q}, \omega)$ of the SS phase along the momentum path $\mathbf{Q}_1 - \Gamma - \mathbf{Q}_2$ in Fig. 4(g), and along $\Gamma - X - M - \Gamma$ in Fig. 4(h). The plots show two spin-wave modes from the spiral order and one mode from the ferromagnetic order with a bandwidth $\sim 13J$. The spin-wave modes from the SS phase follow nearly a parabolic dispersion relation

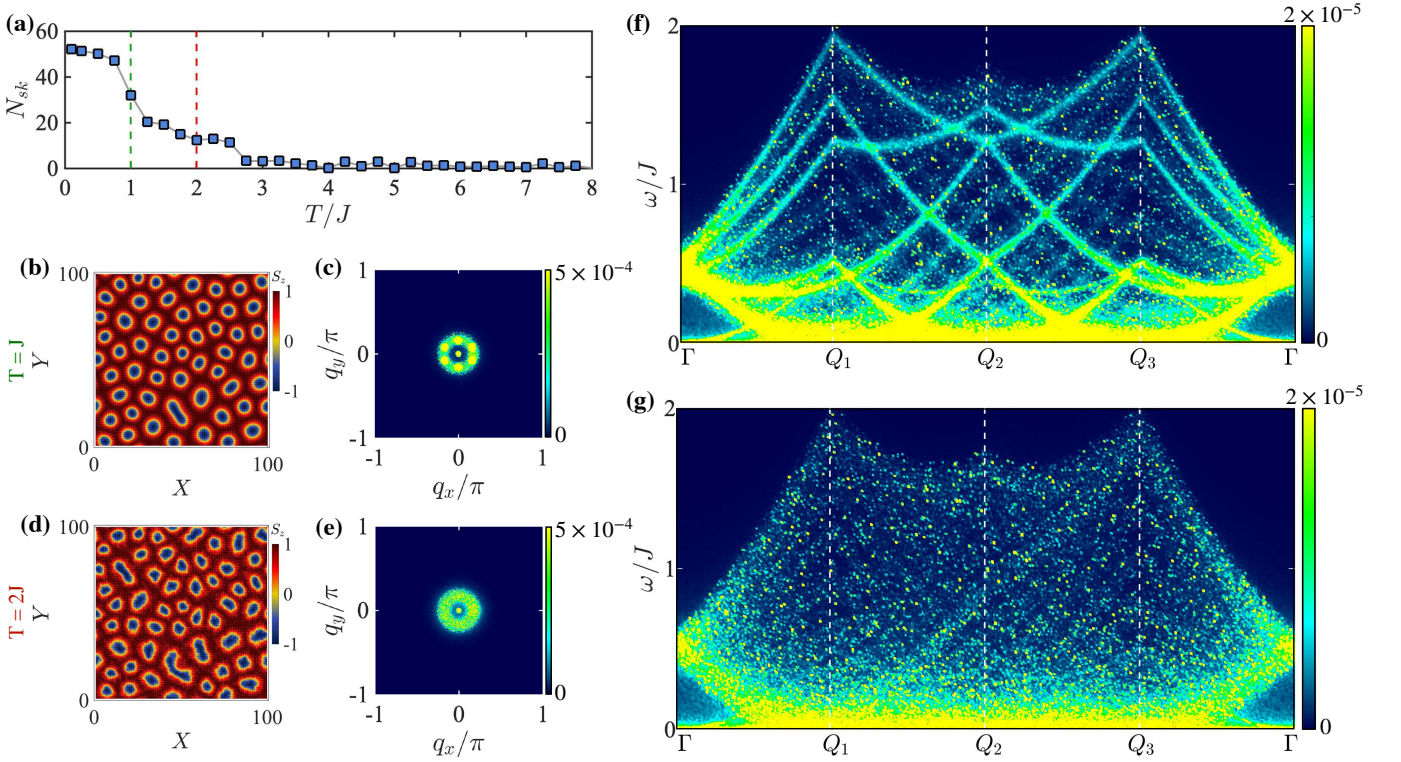


FIG. 5. **Spin waves in the diffusive regime for skyrmion crystallization.** (a) Temperature variation of the skyrmion number N_{sk} , showing the development of the triangular SkX below $T \lesssim 2.5J$. (b), (d) The spin configurations at temperatures (b) $T=J$ and (d) $T=2J$, obtained during an annealing process at a magnetic field $H_z=0.18J$. (c) and (e) are the zero-energy contours of the dynamical spin structure factor $S(\mathbf{q}, \omega)$ at the two temperatures $T=J$ and $T=2J$, respectively. (f), (g) Plots of $S(\mathbf{q}, \omega)$ along the momentum path $\Gamma - \mathbf{Q}_1 - \mathbf{Q}_2 - \mathbf{Q}_3 - \Gamma$ at the two temperatures, representatives of the diffusive regime for the SkX crystallization. Other parameters employed are as in Fig. 1.

($\omega \propto q^2$) in the low-energy regime $\omega \lesssim J$. The two-fold degenerate spin-wave excitation at $\omega \approx 0.8J$ at the Γ point (Fig. 4(g)) is detectable in microwave spectroscopy experiments.

Theoretical calculations [43] and inelastic neutron-scattering experiments in the context of chiral magnets [44, 52, 54–61] analyzed the “helimagnon” excitation modes of the SS phase.

A ferromagnetic spin-wave mode, corresponding to the zero wave-vector magnetic order, is expected to robustly emerge from $\omega=0$ in the case of the conical spin spiral phase, that appears in three-dimensional chiral magnets at zero magnetic field and in two-dimensional oxide interfaces with an in-plane magnetic field [43].

Diffusive regime for skyrmion crystallization. Until now we have discussed the spin-wave excitations of the three stable ground state phases of the considered oxide interface. We now turn our attention to the finite-temperature regime in which the crystallization of the skyrmions takes place as the temperature is lowered down. In our model, the triangular SkX phase is stabilized below a temperature $T_s \lesssim 0.8J$ (which, in Kelvin unit, lies in the range $11 \text{ K} \lesssim T_s \lesssim 35 \text{ K}$, depending on the thickness of the manganite layer), as revealed

by the temperature dependence of the skyrmion number $N_{sk} = \frac{1}{4\pi} \int \mathbf{S} \cdot (\frac{\partial \mathbf{S}}{\partial x} \times \frac{\partial \mathbf{S}}{\partial y}) dx dy$, plotted in Fig. 5(a). However, the development of the skyrmionic correlation begins at temperatures below $T \approx 2.5J$, much above T_s , in the annealing process when the temperature is reduced gradually. The temperature range $0.8J \lesssim T \lesssim 2.5J$ is the weak crystallization regime at the considered values of D and H_z . The snapshots of the spin configuration at two temperatures $T=J$ and $T=2J$ are shown, respectively in Fig. 5(b) and (d). This diffusive regime may also involve an extended skyrmion gas phase, that we explored in our previous study [32]. The constant-energy contour of the dynamical spin structure factor $S(\mathbf{q}, \omega)$ at $\omega=0$ and at temperature $T=2J$, in Fig. 5(e), shows a ring-shaped profile. At the smaller temperature $T=J$, in Fig. 5(c), the six-peak structure, which is a reminiscent of the triangular crystal of skyrmions, appears with the ring in the background. Such a paramagnetic-to-skyrmion lattice transition has been observed in the transition metal helimagnet MnSi using small-angle neutron scattering, neutron-resonance spin-echo spectroscopy, and microwave spectroscopy experiments [49].

Figures 5(f) and (g) show the energy-momentum dependence of $S(\mathbf{q}, \omega)$ along the momentum path $\Gamma - \mathbf{Q}_1 -$

$\mathbf{Q}_2 - \mathbf{Q}_3 - \Gamma$ at the two temperatures $T=J$ and $T=2J$, respectively. At $T=J$, the spin-wave modes of the SkX can be resolved well from the merged background of the diffusively-scattered intensities. On the contrary, at $T=2J$, the ring-shaped elastic profile do not reveal any clear mode of the spin-wave branches. Interestingly, however, the modes near $\omega \approx 0.5J$ at the Γ point persist, despite a smearing in the intensities within a narrow energy range. The measurement of these smeared modes of $S(\mathbf{q}, \omega)$ at zero wave vector can be useful to distinguish the elastic neutron-scattering pattern of a SkX from the nearly-similar one of the hexagonal ferrofluids [62], iron oxide nanoparticles [63], hexagonal magnets [64] and possibly ferromagnetic domains.

The transition from the ring shape to the six-peak structure of elastic $S(\mathbf{q}, \omega)$ profile upon reducing temperature in the diffusive regime, therefore, establishes the fact that fluctuating skyrmionic correlation starts to develop at temperatures much above the SkX-ordering temperature T_s as the precursor of the long-range triangular crystal of skyrmions. Such a precursor phenomenon has been reported in the cubic helimagnets FeGe and MnSi using ac-magnetic susceptibility and magneto-heat capacity measurements [47, 48].

III. DISCUSSION

The presented dynamical spin structure factor of the skyrmion crystal reveals a rich structure of the spin-wave excitations that can be achieved at the manganite/iridate or similar oxide interfaces where a skyrmion crystal is expected to be formed. Its detection in inelastic neutron-scattering experiments can offer an opportunity to effectively probe the topological magnetic textures which is often difficult to deduce conclusively from only the topological Hall effect measurements. The challenge for the successful detection of the SkX spin-wave modes in inelastic scattering experiments lies in obtaining a sufficiently high signal-to-noise ratio from a single interface. For this purpose, multilayer heterostructures, composed of alternate manganite and iridate layers can provide a workable platform. From discussion with experts in the preparation of superlattices, we note that the mass of a typical $\text{La}_{1-x}\text{Sr}_x\text{MnO}_3/\text{SrIrO}_3/\text{SrTiO}_3$ superlattice (of thickness 50 – 75 nm) is ~ 0.003 g, implying that a sample mass of 0.1 g can be achieved by stacking ~ 30 of those superlattices [65]. Considering that LaMnO_3 has a molar mass 239.3 g/mol, a 0.1 g sample contains 0.4 millimoles, while a generic criterion for inelastic neutron scattering experiments is to have samples of about 6.2 (3.5) millimoles for $S=3/2$ ($S=2$) Mn spins. Thus, measurements with these small samples are likely a factor 10 beyond current capabilities, such as the Spallation Neutron Source in the United States, the Institut Laue-Langevin in France, the ISIS neutron source in the United Kingdom, and J-PARC in Japan. There are additional considerations such as neutron absorption, back-

ground from the substrate scattering, bandwidth of the excitations, achieving appropriate coverage in reciprocal space, etc for a successful neutron-scattering experiment. However, such experiments are likely feasible at planned or under construction next generation neutron sources, such as the European Spallation Source or the Second Target Station at the Spallation Neutron Source, where improvements in instrumentation and neutron flux are anticipated to result in performance gains in excess of an order of magnitude [66–68].

Although the challenges related to the thin-film geometry of oxide interfaces are considerable with regards to sample mass, if robust results could be experimentally gathered they will enrich the understanding of the dynamics of the skyrmions which are of high technological interests owing to their potential for wide-spread applications in the high-density data storage [69] and magnonic devices [70]. Another merit of the presented results and the proposed inelastic measurements would be to distinguish the elastic neutron-scattering pattern of a skyrmion crystal from the nearly-similar one of the hexagonal ferrofluids [62], iron oxide nanoparticles [63], and hexagonal magnets [64].

To conclude, we theoretically investigated the spin-wave excitations of a two-dimensional Dzyaloshinskii-Moriya magnet, in the context of the two-dimensional interface between lanthanum manganite and strontium iridate, by computing the dynamical spin structure factor. We explore the excitation modes appearing in the SkX, SS, and FM phases obtained using Monte Carlo simulations and Landau-Lifshitz spin dynamics at different magnetic fields. In particular, we focus on the SkX phase which shows a complex interesting structure in the spin dynamical spin structure factor at low temperatures. We also present the spin-wave excitations in the diffusive regime above the SkX-ordering temperature T_s and show that fluctuating skyrmionic correlation develops at temperatures much above T_s as the precursor of the long-range SkX phase. We finally discussed the possible challenges in the experimental detection and propose a multilayer heterostructure geometry that might overcome some of the obstacles to successfully observe these spin-wave modes from the SkX phase at oxide interfaces.

IV. METHODS

Monte Carlo annealing. We obtain the spin configurations on a square lattice of size 100×100 with periodic boundary conditions using the Monte Carlo (MC) annealing procedure. For all considered magnetic fields, the annealing process was started at a high temperature $T = 30J$ with a completely random spin configuration and the temperature was lowered slowly down to a low value $T = 0.001J$ in 1000 temperature steps. At each temperature, 10^9 MC spin updates were performed. In each spin update step, the spin angle, either the polar angle θ or the azimuthal angle ϕ , was

changed to $\theta \pm 2^\circ$ or $\phi \pm 2^\circ$, respectively (the sign was also chosen randomly) and the new spin configuration was accepted or rejected according to the standard Metropolis algorithm by comparing the total energies of the previous and the new trial spin configurations, calculated using the Hamiltonian in Eq. (1).

Landau-Lifshitz spin dynamics. Starting with the initial conditions obtained from MC simulations at temperature $T = 0.001J$, the spins are integrated numerically and averaged over the initial values using the Landau-Lifshitz equations of motion

$$\frac{d\mathbf{S}_\mathbf{r}(t)}{dt} = \frac{\partial \mathcal{H}}{\partial \mathbf{S}_\mathbf{r}(t)} \times \mathbf{S}_\mathbf{r}(t), \quad (2)$$

where \mathcal{H} is the Hamiltonian described in Eq. (1) and $\mathbf{S}_\mathbf{r}(t)$ is the spin vector at position \mathbf{r} and time t .

The central object of investigation is the dynamical spin structure factor $S(\mathbf{q}, \omega)$, expressed as

$$S(\mathbf{q}, \omega) = \sum_{\alpha, \beta} \left(\delta_{\alpha\beta} - \frac{q_\alpha q_\beta}{q^2 + \eta^2} \right) \times \frac{1}{2\pi N} \sum_{\mathbf{r}, \mathbf{r}'} e^{-i\mathbf{q} \cdot (\mathbf{r} - \mathbf{r}')} \int_{-\infty}^{\infty} dt e^{-i\omega t} C^{\alpha\beta}(\mathbf{r} - \mathbf{r}', t) \quad (3)$$

which is the space-time Fourier transform of the dynamical spin correlation function $C^{\alpha\beta}(\mathbf{r} - \mathbf{r}', t)$

$$C^{\alpha\beta}(\mathbf{r} - \mathbf{r}', t) = \left[\langle S_\mathbf{r}^\alpha(t) S_{\mathbf{r}'}^\beta(0) \rangle - \langle S_\mathbf{r}^\alpha(t) \rangle \langle S_{\mathbf{r}'}^\beta(0) \rangle \right], \quad (4)$$

where α and β represent the x, y , and z components. N is the total number of lattice sites and the parameter $\eta = 0.01$ was used to obtain $S(\mathbf{q}, \omega)$ at $q = 0$. The factor $(\delta_{\alpha\beta} - \frac{q_\alpha q_\beta}{q^2 + \eta^2})$ was used in Eq. (3) to include the off-diagonal components of the correlation function $C^{\alpha\beta}(\mathbf{r} - \mathbf{r}', t)$ ($\alpha \neq \beta$).

While solving Eq. (2), we express the spins using spherical polar coordinates and evaluate the evolution of the polar and the azimuthal angles θ and ϕ . The time integration in Eq. (2) was carried out using the fourth-order Runge-Kutta method to a maximum time $t_{max} = 1000J^{-1}$ with a time step $\Delta t = 0.001J^{-1}$. The finite time cutoff may introduce small oscillations in $S(\mathbf{q}, \omega)$ along the ω axis, resulting from the time Fourier transform. These oscillations were minimized using the convolution of the spin-spin correlation function with a resolution function in frequency, equivalent to the energy resolution of the SANS spectrometer. A Gaussian broadening function with a broadening parameter σ_ω yields the modulated dynamical spin structure factor [51]

$$S(\mathbf{q}, \omega) = \frac{1}{\sqrt{2\pi}\sigma_\omega} \int_{-\infty}^{\infty} S'(\mathbf{q}, \omega') \exp\left[-\frac{(\omega - \omega')^2}{2\sigma_\omega^2}\right] d\omega', \quad (5)$$

where $S'(\mathbf{q}, \omega')$ is the dynamical spin structure factor, calculated using a time cutoff. In the results presented

in this paper, $\sigma_\omega = 0.001J$ was sufficient to resolve different spin-wave modes. $S(\mathbf{q}, \omega)$ was calculated using 50 different realizations of the MC spin configurations and averaged. One advantage of the current approach over linear spin-wave theory techniques is the scope to examine spin dynamics at finite temperatures, where the spin system does not have a well-established long-range order.

ACKNOWLEDGMENTS

The authors acknowledge discussion with Elizabeth M. Skoropata and Ho Nyung Lee on the specification of their manganite-iridate thin films. All members of this collaboration were supported by the U.S. Department of Energy (DOE), Office of Science, Basic Energy Sciences (BES), Materials Sciences and Engineering Division.

REFERENCES

- [1] L. D. Barron, “Chirality and magnetism shake hands,” *Nat. Mater.* **7**, 691 (2008).
- [2] A. Fert, N. Reyren, and V. Cros, “Magnetic skyrmions: advances in physics and potential applications,” *Nat. Rev. Mater.* **2**, 17031 (2017).
- [3] N. Nagaosa and Y. Tokura, “Topological properties and dynamics of magnetic skyrmions,” *Nat. Nanotechnol.* **8**, 899 (2013).
- [4] M. Ezawa, “Compact merons and skyrmions in thin chiral magnetic films,” *Phys. Rev. B* **83**, 100408 (2011).
- [5] S. Buhrandt and L. Fritz, “Skyrmion lattice phase in three-dimensional chiral magnets from Monte Carlo simulations,” *Phys. Rev. B* **88**, 195137 (2013).
- [6] S. Rohart and A. Thiaville, “Skyrmion confinement in ultrathin film nanostructures in the presence of Dzyaloshinskii-Moriya interaction,” *Phys. Rev. B* **88**, 184422 (2013).
- [7] R. Ozawa, S. Hayami, and Y. Motome, “Zero-field skyrmions with a high topological number in itinerant magnets,” *Phys. Rev. Lett.* **118**, 147205 (2017).
- [8] U. K. Röckler, A. N. Bogdanov, and C. Pfleiderer, “Spontaneous skyrmion ground states in magnetic metals,” *Nature* **442**, 797 (2006).
- [9] S. Mühlbauer, B. Binz, F. Jonietz, C. Pfleiderer, A. Rosch, A. Neubauer, R. Georgii, and P. Böni, “Skyrmion lattice in a chiral magnet,” *Science* **323**, 915 (2009).
- [10] X. Z. Yu, Y. Onose, N. Kanazawa, J. H. Park, J. H. Han, Y. Matsui, N. Nagaosa, and Y. Tokura, “Real-space observation of a two-dimensional skyrmion crystal,” *Nature* **465**, 901 (2010).
- [11] X. Z. Yu, N. Kanazawa, Y. Onose, K. Kimoto, W. Z. Zhang, S. Ishiwata, Y. Matsui, and Y. Tokura, “Near room-temperature formation of a skyrmion crystal in thin-films of the helimagnet FeGe,” *Nat. Mater.* **10**, 106 (2011).
- [12] S. Heinze, K. von Bergmann, M. Menzel, J. Brede, A. Kubetzka, R. Wiesendanger, G. Bihlmayer, and S. Blügel, “Spontaneous atomic-scale magnetic skyrmion lattice in two dimensions,” *Nat. Phys.* **7**, 713 (2011).

- [13] X. Z. Yu, Y. Tokunaga, Y. Kaneko, W. Z. Zhang, K. Kimoto, Y. Matsui, Y. Taguchi, and Y. Tokura, “Biskyrmion states and their current-driven motion in a layered manganite,” *Nat. Commun.* **5**, 3198 (2014).
- [14] H. S. Park, X. Yu, S. Aizawa, T. Tanigaki, T. Akashi, Y. Takahashi, T. Matsuda, N. Kanazawa, Y. Onose, D. Shindo, A. Tonomura, and Y. Tokura, “Observation of the magnetic flux and three-dimensional structure of skyrmion lattices by electron holography,” *Nat. Nanotechnol.* **9**, 337 (2014).
- [15] S. Woo, K. Litzius, B. Krüger, M.-Y. Im, L. Caretta, K. Richter, M. Mann, A. Krone, R. M. Reeve, M. Weigand, P. Agrawal, I. Lemesch, M.-A. Mawass, P. Fischer, M. Kläui, and G. S. D. Beach, “Observation of room-temperature magnetic skyrmions and their current-driven dynamics in ultrathin metallic ferromagnets,” *Nat. Mater.* **15**, 501 (2016).
- [16] M. Hervé, B. Dupé, R. Lopes, M. Böttcher, M. D. Martins, T. Balashov, L. Gerhard, J. Sinova, and W. Wulfhekel, “Stabilizing spin spirals and isolated skyrmions at low magnetic field exploiting vanishing magnetic anisotropy,” *Nat. Commun.* **9**, 1015 (2018).
- [17] S. Mühlbauer, D. Honecker, É. A. Périgo, F. Bergner, S. Disch, A. Heinemann, S. Erokhin, D. Berkov, C. Leighton, M. R. Eskildsen, and A. Michels, “Magnetic small-angle neutron scattering,” *Rev. Mod. Phys.* **91**, 015004 (2019).
- [18] T. Schulz, R. Ritz, A. Bauer, M. Halder, M. Wagner, C. Franz, C. Pfleiderer, K. Everschor, M. Garst, and A. Rosch, “Emergent electrodynamics of skyrmions in a chiral magnet,” *Nat. Phys.* **8**, 301 (2012).
- [19] N. Nagaosa, X. Z. Yu, and Y. Tokura, “Gauge fields in real and momentum spaces in magnets: monopoles and skyrmions,” *Phil. Trans. R. Soc. A* **370**, 5806 (2012).
- [20] A. Neubauer, C. Pfleiderer, B. Binz, A. Rosch, R. Ritz, P. G. Niklowitz, and P. Böni, “Topological Hall effect in the A phase of MnSi,” *Phys. Rev. Lett.* **102**, 186602 (2009).
- [21] N. Kanazawa, Y. Onose, T. Arima, D. Okuyama, K. Ohoyama, S. Wakimoto, K. Kakurai, S. Ishiwata, and Y. Tokura, “Large topological Hall effect in a short-period helimagnet MnGe,” *Phys. Rev. Lett.* **106**, 156603 (2011).
- [22] Y. Taguchi, Y. Oohara, H. Yoshizawa, N. Nagaosa, and Y. Tokura, “Spin chirality, Berry phase, and anomalous Hall effect in a frustrated ferromagnet,” *Science* **291**, 2573 (2001).
- [23] S. X. Huang and C. L. Chien, “Extended skyrmion phase in epitaxial FeGe(111) thin films,” *Phys. Rev. Lett.* **108**, 267201 (2012).
- [24] K. G. Rana, O. Meshcheriakova, J. Kübler, B. Ernst, J. Karel, R. Hillebrand, E. Pippel, P. Werner, A. K. Nayak, C. Felser, and S. S. P. Parkin, “Observation of topological Hall effect in Mn₂RhSn films,” *New J. Phys.* **18**, 085007 (2016).
- [25] L. Wang, Q. Feng, Y. Kim, R. Kim, K. H. Lee, S. D. Pollard, Y. J. Shin, H. Zhou, W. Peng, D. Lee, W. Meng, H. Yang, J. H. Han, M. Kim, Q. Lu, and T. W. Noh, “Ferroelectrically tunable magnetic skyrmions in ultrathin oxide heterostructures,” *Nat. Mater.* **17**, 1087 (2018).
- [26] K. Hamamoto, M. Ezawa, and N. Nagaosa, “Quantized topological Hall effect in skyrmion crystal,” *Phys. Rev. B* **92**, 115417 (2015).
- [27] S. D. Yi, S. Onoda, N. Nagaosa, and J. H. Han, “Skyrmions and anomalous Hall effect in a Dzyaloshinskii-Moriya spiral magnet,” *Phys. Rev. B* **80**, 054416 (2009).
- [28] M. Nakamura, D. Morikawa, X. Yu, F. Kagawa, T. Arima, Y. Tokura, and M. Kawasaki, “Emergence of topological Hall effect in half-metallic manganite thin films by tuning perpendicular magnetic anisotropy,” *J. Phys. Soc. Jpn.* **87**, 074704 (2018).
- [29] P. Swekis, A. Markou, D. Kriegner, J. Gayles, R. Schlitz, W. Schnelle, S. T. B. Goennenwein, and C. Felser, “Topological Hall effect in thin films of Mn_{1.5}PtSn,” *Phys. Rev. Materials* **3**, 013001 (2019).
- [30] P. Vir, J. Gayles, A. S. Sukhanov, N. Kumar, F. Damay, Yan Sun, J. Kübler, C. Shekhar, and C. Felser, “Anisotropic topological Hall effect with real and momentum space Berry curvature in the antiskyrmion-hosting Heusler compound Mn_{1.4}PtSn,” *Phys. Rev. B* **99**, 140406 (2019).
- [31] N. Mohanta, S. Okamoto, and E. Dagotto, “Planar Topological Hall Effect from Conical Spin Spirals,” *arXiv:1911.02978* (2019).
- [32] N. Mohanta, E. Dagotto, and S. Okamoto, “Topological Hall effect and emergent skyrmion crystal at manganite-iridate oxide interfaces,” *Phys. Rev. B* **100**, 064429 (2019).
- [33] J. Nichols, X. Gao, S. Lee, T. L. Meyer, J. W. Freeland, V. Lauter, D. Yi, J. Liu, D. Haskel, J. R. Petrie, E.-J. Guo, A. Herklotz, D. Lee, T. Z. Ward, G. Eres, M. R. Fitzsimmons, and H. N. Lee, “Emerging magnetism and anomalous Hall effect in iridate-manganite heterostructures,” *Nat. Commun.* **7**, 12721 (2016).
- [34] S. Okamoto, J. Nichols, C. Sohn, S. Y. Kim, T. W. Noh, and H. N. Lee, “Charge transfer in iridate-manganite superlattices,” *Nano Lett.* **17**, 2126 (2017).
- [35] X. Li, W. V. Liu, and L. Balents, “Spirals and skyrmions in two dimensional oxide heterostructures,” *Phys. Rev. Lett.* **112**, 067202 (2014).
- [36] S. Banerjee, O. Erten, and M. Randeria, “Ferromagnetic exchange, spin-orbit coupling and spiral magnetism at the LaAlO₃/SrTiO₃ interface,” *Nat. Phys.* **9**, 626 (2013).
- [37] J. Matsuno, N. Ogawa, K. Yasuda, F. Kagawa, W. Koshibae, N. Nagaosa, Y. Tokura, and M. Kawasaki, “Interface-driven topological Hall effect in SrRuO₃-SrIrO₃ bilayer,” *Sci. Adv.* **2**, e1600304 (2016).
- [38] L. Vistoli, W. Wang, A. Sander, Q. Zhu, B. Casals, R. Cichelero, A. Barthélémy, S. Fusil, G. Herranz, S. Valencia, R. Abrudan, E. Weschke, K. Nakazawa, H. Kohno, J. Santamaria, W. Wu, V. Garcia, and M. Bibes, “Giant topological Hall effect in correlated oxide thin films,” *Nat. Phys.* **15**, 67 (2019).
- [39] Y. Li, L. Zhang, Q. Zhang, C. Li, T. Yang, Y. Deng, L. Gu, and D. Wu, “Emergent Topological Hall Effect in La_{0.7}Sr_{0.3}MnO₃/SrIrO₃ Heterostructures,” *ACS Appl. Mater. Interfaces* **11**, 21268 (2019).
- [40] R. D. Desautels, L. DeBeer-Schmitt, S. A. Montoya, J. A. Borchers, S.-G. Je, N. Tang, M.-Y. Im, M. R. Fitzsimmons, E. E. Fullerton, and D. A. Gilbert, “Realization of ordered magnetic skyrmions in thin films at ambient conditions,” *Phys. Rev. Materials* **3**, 104406 (2019).
- [41] M. Mochizuki, “Spin-Wave Modes and Their Intense Excitation Effects in Skyrmion Crystals,” *Phys. Rev. Lett.* **108**, 017601 (2012).

- [42] O. Petrova and O. Tchernyshyov, “Spin waves in a skyrmion crystal,” *Phys. Rev. B* **84**, 214433 (2011).
- [43] M. Garst, J. Waizner, and D. Grundler, “Collective spin excitations of helices and magnetic skyrmions: review and perspectives of magnonics in non-centrosymmetric magnets,” *Journal of Physics D: Applied Physics* **50**, 293002 (2017).
- [44] T. Schwarze, J. Waizner, M. Garst, A. Bauer, I. Stasinopoulos, H. Berger, C. Pfleiderer, and D. Grundler, “Universal helimagnon and skyrmion excitations in metallic, semiconducting and insulating chiral magnets,” *Nat. Mater.* **14**, 478 (2015).
- [45] Y. Onose, Y. Okamura, S. Seki, S. Ishiwata, and Y. Tokura, “Observation of magnetic excitations of skyrmion crystal in a helimagnetic insulator Cu_2OSeO_3 ,” *Phys. Rev. Lett.* **109**, 037603 (2012).
- [46] D. Ehlers, I. Stasinopoulos, V. Tsurkan, H.-A. Krug von Nidda, T. Fehér, A. Leonov, I. Kézsmárki, D. Grundler, and A. Loidl, “Skyrmion dynamics under uniaxial anisotropy,” *Phys. Rev. B* **94**, 014406 (2016).
- [47] H. Wilhelm, M. Baenitz, M. Schmidt, U. K. Röfller, A. A. Leonov, and A. N. Bogdanov, “Precursor phenomena at the magnetic ordering of the cubic helimagnet FeGe,” *Phys. Rev. Lett.* **107**, 127203 (2011).
- [48] S. Shanmukharao Samatham and V. Ganesan, “Precursor state of skyrmions in MnSi: a heat capacity study,” *Phys. Status Solidi* **7**, 184 (2013).
- [49] J. Kindervater, I. Stasinopoulos, A. Bauer, F. X. Haslbeck, F. Rucker, A. Chacon, S. Mühlbauer, C. Franz, M. Garst, D. Grundler, and C. Pfleiderer, “Weak Crystallization of Fluctuating Skyrmion Textures in MnSi,” *Phys. Rev. X* **9**, 041059 (2019).
- [50] S. Banerjee, J. Rowland, O. Erten, and M. Randeria, “Enhanced stability of skyrmions in two-dimensional chiral magnets with Rashba spin-orbit coupling,” *Phys. Rev. X* **4**, 031045 (2014).
- [51] K. Chen and D. P. Landau, “Spin-dynamics study of the dynamic critical behavior of the three-dimensional classical heisenberg ferromagnet,” *Phys. Rev. B* **49**, 3266 (1994).
- [52] S. V. Grigoriev, A. S. Sukhanov, E. V. Altynbaev, S.-A. Siegfried, A. Heinemann, P. Kizhe, and S. V. Maleyev, “Spin waves in full-polarized state of Dzyaloshinskii-Moriya helimagnets: Small-angle neutron scattering study,” *Phys. Rev. B* **92**, 220415 (2015).
- [53] F. J. dos Santos, M. dos Santos Dias, F. S. M. Guimarães, J. Bouaziz, and S. Lounis, “Spin-resolved inelastic electron scattering by spin waves in noncollinear magnets,” *Phys. Rev. B* **97**, 024431 (2018).
- [54] M. Kugler, G. Brandl, J. Waizner, M. Janoschek, R. Georgii, A. Bauer, K. Seemann, A. Rosch, C. Pfleiderer, P. Böni, and M. Garst, “Band Structure of Helimagnons in MnSi Resolved by Inelastic Neutron Scattering,” *Phys. Rev. Lett.* **115**, 097203 (2015).
- [55] A. Dussaux, P. Schoenherr, K. Koumpouras, J. Chico, K. Chang, L. Lorenzelli, N. Kanazawa, Y. Tokura, M. Garst, A. Bergman, C. L. Degen, and D. Meier, “Local dynamics of topological magnetic defects in the itinerant helimagnet FeGe,” *Nat. Commun.* **7**, 12430 (2016).
- [56] G. S. Tucker, J. S. White, J. Romhányi, D. Szaller, I. Kézsmárki, B. Roessli, U. Stuhr, A. Magrez, F. Groitl, P. Babkevich, P. Huang, I. Živković, and H. M. Rønnow, “Spin excitations in the skyrmion host Cu_2OSeO_3 ,” *Phys. Rev. B* **93**, 054401 (2016).
- [57] P. Y. Portnichenko, J. Romhányi, Y. A. Onyikienko, A. Henschel, M. Schmidt, A. S. Cameron, M. A. Surmach, J. A. Lim, J. T. Park, A. Schneidewind, D. L. Abernathy, H. Rosner, Jeroen van den Brink, and D. S. Inosov, “Magnon spectrum of the helimagnetic insulator Cu_2OSeO_3 ,” *Nat. Commun.* **7**, 10725 (2016).
- [58] A. Bauer, A. Chacon, M. Wagner, M. Halder, R. Georgii, A. Rosch, C. Pfleiderer, and M. Garst, “Symmetry breaking, slow relaxation dynamics, and topological defects at the field-induced helix reorientation in MnSi,” *Phys. Rev. B* **95**, 024429 (2017).
- [59] E. Turgut, A. Park, K. Nguyen, A. Moehle, D. A. Muller, and G. D. Fuchs, “Chiral magnetic excitations in FeGe films,” *Phys. Rev. B* **95**, 134416 (2017).
- [60] S.-A. Siegfried, A. S. Sukhanov, E. V. Altynbaev, D. Honecker, A. Heinemann, A. V. Tsvyashchenko, and S. V. Grigoriev, “Spin-wave dynamics in the helimagnet FeGe studied by small-angle neutron scattering,” *Phys. Rev. B* **95**, 134415 (2017).
- [61] M. Weiler, A. Aqeel, M. Mostovoy, A. Leonov, S. Geprägs, R. Gross, H. Huebl, T. T. M. Palstra, and S. T. B. Goennenwein, “Helimagnon resonances in an intrinsic chiral magnonic crystal,” *Phys. Rev. Lett.* **119**, 237204 (2017).
- [62] C. Gollwitzer, I. Rehberg, and R. Richter, “Via hexagons to squares in ferrofluids: experiments on hysteretic surface transformations under variation of the normal magnetic field,” *J. Phys. Condens. Matter* **18**, S2643 (2006).
- [63] Z. Fu, Y. Xiao, A. Feoktystov, V. Pipich, M.-S. Appavou, Y. Su, E. Feng, W. Jin, and T. Brückel, “Field-induced self-assembly of iron oxide nanoparticles investigated using small-angle neutron scattering,” *Nanoscale* **8**, 18541. (2016).
- [64] R. Takagi, J. S. White, S. Hayami, R. Arita, D. Honecker, H. M. Rønnow, Y. Tokura, and S. Seki, “Multiple-q non-collinear magnetism in an itinerant hexagonal magnet,” *Sci. Adv.* **4** (2018).
- [65] Personal communication with Elizabeth M. Skoropata and Ho Nyung Lee.
- [66] “First experiments: New science opportunities at the spallation neutron source second target statio,” Access Date: 2020-05-13.
- [67] “Instruments: European spallation source,” Access Date: 2020-05-13.
- [68] “Cold chopper spectrometer: European spallation source,” Access Date: 2020-05-13.
- [69] K. Everschor-Sitte, J. Masell, R. M. Reeve, and M. Kläui, “Perspective: Magnetic skyrmions—overview of recent progress in an active research field,” *J. Appl. Phys.* **124**, 240901 (2018).
- [70] F. Ma, Y. Zhou, H. B. Braun, and W. S. Lew, “Skyrmion-based dynamic magnonic crystal,” *Nano Lett.* **15**, 4029 (2015).